

# Layer-by-Layer Film Growth Using Polysaccharides and Recombinant Polypeptides: A Combinatorial Approach

Rui R. Costa,<sup>†,‡</sup> Ana M. Testera,<sup>§,||</sup> F. Javier Arias,<sup>§,||</sup> J. Carlos Rodríguez-Cabello,<sup>§,||</sup> and João F. Mano<sup>\*,†,‡</sup>

<sup>†</sup>University of Minho, 3B's Research Group – Biomaterials, Biodegradables and Biomimetics, Headquarters of the European Institute of Excellence on Tissue Engineering and Regenerative Medicine, Avepark, 4806-909 Caldas das Taipas, Guimarães, Portugal

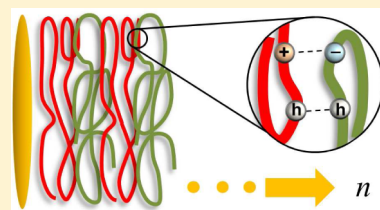
<sup>‡</sup>ICVS/3B's, PT Government Associated Laboratory, Braga/Guimarães, Portugal

<sup>§</sup>University of Valladolid, G.I.R. Bioforge, Edificio I + D, Paseo de Belén, 1, 47011, Valladolid, Spain

<sup>||</sup>Networking Research Center on Bioengineering, Biomaterials and Nanomedicine (CIBER-BBN), Valladolid, Spain

## Supporting Information

**ABSTRACT:** Nanostructured films consisting of polysaccharides and elastin-like recombinamers (ELRs) are fabricated in a layer-by-layer manner. A quartz-crystal microbalance with dissipation monitoring (QCM-D) is used to follow the buildup of hybrid films containing one polysaccharide (chitosan or alginate) and one of several ELRs that differ in terms of amino acid content, length, and biofunctionality *in situ* at pH 4.0 and pH 5.5. The charge density of the ingredients at each pH is determined by measuring their  $\zeta$ -potential, and the thickness of a total of 36 different films containing five bilayers is estimated using the Voigt-based viscoelastic model. A comparison of the values obtained reveals that thicker films can be obtained when working at a pH close to the acidity constant of the polysaccharide used (near- $pK_a$  conditions), suggesting that the construction of such films is more favorable when based on the presence of hydrophobic interactions between ELRs and partially neutralized polysaccharides. Further analysis shows that the molecular weight of the ELRs plays only a minor role in defining the growth tendency. When taken together, these results point to the most favorable conditions for constructing nanostructured films from natural and distinct recombinant polypeptides that can be tuned to exhibit specialized biofunctionality for tissue-engineering, drug-delivery, and biotechnological applications.



## INTRODUCTION

Surface engineering is a field of expertise concerned with the modification and improvement of interfaces.<sup>1–3</sup> In the past decades, this technique has been widely applied in the field of biomedical and tissue engineering, where the properties of substrate surfaces need to be tuned to promote cell expansion, improve the interface between an implantable device and its biological environment, and add stimuli-responsiveness for on-demand surface property switching.<sup>4–7</sup> Layer-by-layer (LbL) techniques are perhaps the most versatile and easy-to-apply of the numerous surface-modification tools currently available as they are based on the spontaneous adsorption of ingredients onto a substrate, generally a polymer, biomolecule, or inorganic particle, and allow the sequential formation of a nanostructured film. This technique allows robust coatings to be produced on substrates with complex geometries and, as it does away with the need for harmful organic solvents, it is of great interest in tissue-engineering applications.<sup>5,8–10</sup> As such, LbL methods have already been employed in cell-sheet technology,<sup>11,12</sup> for drug delivery,<sup>13–15</sup> and for the creation of three-dimensional scaffolds for cell culture.<sup>16</sup>

Exploiting strong, long-range electrostatic interactions (e.g., attraction between oppositely charged polyelectrolytes)<sup>17</sup> is by far the most widely used LbL construction mechanism, often referred to as electrostatic self-assembly (ESA). LbL synthesis is not restricted to this mechanism: this technique relies on the

existence of multiple complementary intermolecular interactions that allow the LbL concept to be widened to include hydrogen bonding and hydrophobic interactions (often referred to as secondary or nonelectrostatic interactions).<sup>18–20</sup> Nowadays, it is assumed that the gain in entropy is also a key phenomenon for LbL construction which results from the release of counterions. The outcome of such a mechanism is often the organization of the layers in a more coiled and interdigitated conformation and loss of degrees of freedom from the polyelectrolyte molecules.<sup>19–21</sup>

Herein we intend to demonstrate the feasibility of LbL synthesis using natural marine-based polysaccharides [chitosan (CHI) and alginate (ALG)] and nature-inspired polypeptides, in this case elastin-like recombinamers (ELRs), which are the recombinant analogs of elastin-like polymers (ELPs). The polycationic chitosan and polyanionic alginate are well-known polysaccharides derived from marine crustaceans and brown algae, respectively.<sup>22</sup> Both polymers are nontoxic and exhibit adhesive, bacteriostatic, fungistatic, hemostatic, and antimicrobial effects that make them suitable for use in wound dressings and drug-delivery systems.<sup>23–25</sup> ELRs are genetically modified biocompatible and stimuli-responsive polypeptides that mimic

**Received:** March 22, 2013

**Revised:** May 6, 2013



natural elastin, the extracellular elastic protein found in higher classes of animals.<sup>26–28</sup> These polypeptides exhibit a transition temperature ( $T_t$ ) in aqueous solution above which free polymer chains adopt random coil conformations and separate from the solvent. ELRs follow the standard repeating structure of elastin, namely, valine-proline-glycine-valine-glycine, (VPGVG), a sequence with no electrostatic charge. Besides their smart nature, the most attractive property of ELRs is their ability to be engineered to contain amino acid sequences with charge and even bioactivity. Indeed, it has proven possible to construct ELRs containing sequences that enhance cell adhesion<sup>29,30</sup> or biomineralization.<sup>31</sup> One could thus consider that such materials may be able to act as versatile and fine-tuned models for protein systems, including nanostructured coatings for highly specific tissue-engineering applications.

A great deal of time and effort has been dedicated to the widely investigated poly(styrene sulfonate)/poly(allylamine hydrochloride) (PSS/PAH) system, which is currently considered to be a model of how multilayered thin films are built, over the past 20 years.<sup>5</sup> The fact that most studies in this field have been based on the application of ESA interactions to synthetic materials with controllable properties has hindered a more in-depth understanding of the secondary construction mechanism. As a consequence, extrapolation to new tailored materials that are more suitable for tissue-engineering applications, as is the case for ELRs or proteins in general, has been limited. In this regard, classical ESA has been unable to explain fully the formation of multilayer thin films, and the role of secondary interactions has been brought into question. A report from Cini and co-workers—to which also contributed Decher, one of the pioneers of LbL—has also proposed that the construction of poly(allylamine hydrochloride) (PAH) and poly(sodium phosphate) (PSP) “violates almost all the rules” of LbL, thereby suggesting a possible contribution from hydrophobic interactions.<sup>32</sup> Our group has also considered that the formation of an ELR-containing multilayer film is almost certainly driven, at least in part, by hydrophobic interactions.<sup>29</sup> However, to the best of our knowledge, studies that could systematically and extensively confirm the role of such interactions in the construction of multilayered films have yet not been reported.

In this work we intended to study the conditions needed to successfully obtain a hybrid, biomimetic LbL film that combines the properties of natural and genetically modified polymers. We resorted to a quartz-crystal microbalance with dissipation monitoring (QCM-D), a technique that is able to detect adsorbed surface density changes in the order of  $\text{ng}\cdot\text{cm}^{-2}$  and measure the viscoelastic properties of the resulting surface in real time. Based on the piezoelectric effect, QCM has proven to be a powerful technique for evaluating the growth of multilayer films as well as for monitoring the effect of factors such as concentration, molecular weight, and pH during or after their assembly.<sup>33–37</sup> Thus, our objectives were (i) to study the influence of ESA and secondary interactions in the buildup mechanism of the proposed hybrid films by means of charge variations dependent on pH, (ii) study the influence of distinct ELR molecular weights ( $M_n$ ), (iii) compare the feasibility of the construction when using two distinct polysaccharides, CHI and ALG, and (iv) extend the knowledge of LbL mechanisms to the class of ELRs.

## EXPERIMENTAL SECTION

**Materials.** Medium molecular weight chitosan was purchased from Sigma-Aldrich (reference 448877, Brookshield viscosity 200–800 cP, molecular weight 190–310 kDa) and purified by a series of filtering steps and precipitation from water and ethanol, followed by freeze-drying. To determine the degree of deacetylation of chitosan, hydrogen-1 nuclear magnetic resonance ( $^1\text{H}$  NMR) was performed using a Varian MR-400 spectrometer. Ten mg of chitosan was dissolved in 1 mL of deuterated water ( $\text{D}_2\text{O}$ ) and 20  $\mu\text{L}$  of deuterated hydrochloric acid (DCl). An aliquot of this solution was placed in a 5 mm NMR tube and the spectrum recorded at 60  $^\circ\text{C}$ . The calculation method of DD was described elsewhere<sup>38</sup> and was determined to be 82%. Alginate (alginic acid sodium salt from brown algae) was purchased from Fluka (reference 71238, molecular weight 100–200 kDa). ELRs were obtained by the induced gene expression of recombinant *Escherichia coli* strains containing the expressing gene. Each ELR was induced in a 12 L Applikon fermenter, in terrific broth medium (TB) supplemented with carbenicillin (0.1% v/v) and glucose (0.1% v/v), under controlled conditions of temperature (37  $^\circ\text{C}$ ) and pH (7.00). Fermentation was stopped after registering an optical density variation at 600 nm of less than 0.25, in a time frame of 1 h. The culture was then harvested by centrifugation, resuspended, and lysed by ultrasonic disruption. Insoluble debris was removed by centrifugation and the cleared lysate was subjected to several cycles of cold and warm centrifugations (4 and 40  $^\circ\text{C}$ , respectively). All purification steps were carried out in sodium chloride solution (0.5 M). The polymer in solution was dialyzed against ultrapure water, frozen at  $-24$   $^\circ\text{C}$ , and freeze-dried.

**Assessment of the ELR Compositions.** The molecular weight and amino acid composition of the samples obtained were determined by matrix-assisted laser desorption/ionization time-of-flight mass spectroscopy (MALDI-TOF) and amino acid content analysis, respectively. These methods, and their results, are described in more detail in the Supporting Information. The percentage of residues subject to ionization and the proportion of positive and negative charges were also calculated.

**Measurement of the Charges.** The  $\zeta$ -potentials of the polysaccharides and ELRs were determined using a Nano-ZS from Malvern (United Kingdom), at 25  $^\circ\text{C}$ . Aqueous solutions of each ingredient were used, at 100  $\mu\text{g}\cdot\text{mL}^{-1}$ , 0.15 M NaCl, and pH values of 4.0 or 5.5.

**Construction of Hybrid Self-Assembled Films.** A Q-Sense E4 quartz-crystal microbalance (Q-Sense AB, Sweden) with dissipation monitoring system was used to monitor the adsorption of polysaccharides and ELRs onto gold-coated quartz crystals *in situ* (Q-Sense, reference QSX301). The assembled films consisted of a series of polysaccharide/ELR combinations at pH values of either 4.0 or 5.5, thus resulting in a total of 36 different conditions. Combinations containing chitosan had this polycation as the first layer, whereas those containing alginate had this polyanion as the second layer. The quartz-crystal was excited at multiple overtones (1, 3, 5, 7, 9, 11, and 13, corresponding to 5, 15, 25, 35, 45, 55, and 65 MHz, respectively). Adsorption took place at 25  $^\circ\text{C}$ , using solutions at 100  $\mu\text{g}\cdot\text{mL}^{-1}$ , 0.15 M NaCl, and at a constant flow rate of 50  $\text{mL}\cdot\text{min}^{-1}$ , with an adsorption time of 15 min and an intermediate rinsing step of 10 min.

**Table 1.** List of ELRs Used in This Work with Their Corresponding Theoretical Molecular Weight and Proportions of Charged and Positive/Negative Amino Acids<sup>a</sup>

ELR acronym	sequence	$M_n$ (Da)	charged proportion (%)	positive/ negative amino acid proportion (%)
3K-VRDG <sup>(-)</sup> V	MGKKKP-(VPGVG) <sub>14</sub> [(VPGIG) <sub>10</sub> AVTGRDGPASS (VPGIG) <sub>10</sub> ] <sub>2</sub> (VPGVG) <sub>14</sub> -V	31371	1.9	71.4/28.6
3K-VRGDV	MGKKKP(VPGVG) <sub>14</sub> [(VPGIG) <sub>10</sub> AVTGRDGPASS (VPGIG) <sub>10</sub> ] <sub>2</sub> (VPGVG) <sub>14</sub> -V	31371	1.9	71.4/28.6
HAP3	MESLLP[[[(VPGIG) <sub>2</sub> (VPGKG)(VPGIG) <sub>2</sub> DDDEEKFLRRIGRFG[(VPGIG) <sub>2</sub> (VPGKG)(VPGIG) <sub>2</sub> ] <sub>3</sub> ]-V	31877	11.4	60/40
GEG15	MD[(VPGVG) <sub>2</sub> (VPGEG) (VPGVG) <sub>2</sub> ] <sub>15</sub> IGSG	31948	3.9	4/96
H3A20	MESLLP[[[(VPGIG) <sub>2</sub> VPGKG(VPGIG) <sub>2</sub> DDDEEKFLRRIGRFG[(VPGIG) <sub>2</sub> VPGKG(VPGIG) <sub>2</sub> ] <sub>3</sub> ](VPAVG) <sub>20</sub> -V	40361	8.8	60/40
IK24	MESLLP[(VPGIG) <sub>2</sub> (VPGKG)(VPGIG) <sub>2</sub> ] <sub>24</sub> -V	51970	4.0	100/0
H-RGD6	MGSSHHHHHSSGLVPRGSHMESLLP[[[(VPGIG) <sub>2</sub> (VPGKG) (VPGIG) <sub>2</sub> AVTGRDGPASS[(VPGIG) <sub>2</sub> (VPGKG) (VPGIG) <sub>2</sub> ] <sub>6</sub> ]-V	60661	6.4	84.4/15.6
H3A20H3	MESLLP[[[(VPGIG) <sub>2</sub> (VPGKG)(VPGIG) <sub>2</sub> DDDEEKFLRRIGRFG[(VPGIG) <sub>2</sub> (VPGKG) (VPGIG) <sub>2</sub> ] <sub>3</sub> ](VPAVG) <sub>20</sub> [[[(VPGIG) <sub>2</sub> (VPGKG)(VPGIG) <sub>2</sub> DDDEEKFLRRIGRFG[(VPGIG) <sub>2</sub> (VPGKG) (VPGIG) <sub>2</sub> ] <sub>3</sub> ]-V	71462	9.9	60.8/39.2
Neutralized V84	MGK*K*K*P-(VPGVG) <sub>84</sub> -V	35191	0	0/0

<sup>a</sup>\*Neutralized lysine residues.

**Estimation of the Film Thicknesses.** The Voigt-based viscoelastic model contained in the *QTools* software from Q-Sense (version 3.0.15.553) was used to estimate the thickness of the films from the QCM-D monitoring data. Iterations of the model were performed using at least three overtones. The model requires three parameters, namely, solvent density, solvent viscosity, and film density, to be fixed. The solvent viscosity was therefore fixed at 0.001 Pa.s (same as water) and the film density at 1200 kg.m<sup>-3</sup> (often assumed to return the lowest calculation error).<sup>29,37,39</sup> The solvent density was varied by trial and error between 1000 and 1060 kg.m<sup>-3</sup> until the total error,  $\chi^2$ , was minimized.

## RESULTS AND DISCUSSION

**Characterization of the Polysaccharides and ELRs.** We selected nine ELRs for this study as the genetically engineered origin of these compounds allows a class of materials that can differ in terms of sequence, length, and bioactivity without significantly altering the original elastin backbone to be studied. The properties of each ELR are summarized in Table 1 according to their molecular weight,  $M_n$ , amino acid sequence, and proportions of charged/uncharged and positive/negative residues. The acronyms were assigned on the basis of their distinct sequence, function, and variations on the repeating (VPGVG) sequence. The experimental amino acid composition and MALDI-TOF values can be found in Supporting Information (Table S1, Table S2, Table S3, Figure S1) showing that the experimental molecular weight ( $M_n$ ) and number of amino acids agree well with the theoretical values of Table 1. Arginine (R), histidine (H), and lysine (K) are positively charged when protonated, and aspartic acid (D) and glutamic acid (E) are negatively charged when deprotonated. The properties of these residues were taken into account when calculating the charged and amino acid proportions. A closer look at each ELR sequence shows that they are all distinct and some even exhibit motifs with biological relevance that could make them useful for current therapies and applications: 3K-VRGDV and H-RGD6, for example, contain the RGD sequence, which promotes cell adhesion. 3K-VRDG<sup>(-)</sup>V is the negative control of the former as it contains the same sequence but with a scrambled, nonfunctional RDG motif. Similarly, HAP3, H3A20, and H3A20H3 exhibit sequences that promote biomineralization, organized as single, double, and triple blocks,

respectively, with the alanine-block (A20 portion) being highly hydrophobic. GEG15 and IK24 contain E and K residues, which confer anionic and cationic behavior, respectively. Finally, the neutralized V84 lacks ionizable residues and is therefore uncharged. Although the original sequence of V84 contains three K-residues, which in theory should confer a positive charge on this ELR, it was neutralized in order to use it as a neutral control (see Supporting Information, “neutralization of V84”). This sequence was used to analyze the buildup of a neutral ELR hybrid film in comparison with ELRs that are susceptible to ionization.

Like most proteins, the ionizable residues in the backbone of these ELRs represent only a small fraction of the whole sequence (maximum of 11.4% in the case of HAP3). Therefore, although ELRs can be modified to include specific peptide sequences, they still retain the basic properties of this class of polymers. This is a relevant property for the present study, considering that the nonionizable residues may interact by hydrophobic interactions. Despite the fact that these interactions are weaker and have a shorter range than their electrostatic counterparts, they nevertheless have been shown to play an important role in stabilizing the internal structure of multilayers containing uncharged groups, such as most proteins, which contain large numbers of hydrophobic groups.<sup>40–42</sup> Using a group of ELRs with such distinct properties, we expected to be able to identify the properties that are essential for the construction of this kind of hybrid nanostructured film, especially films containing complex ELRs with bioactivity and practical relevance.

**Effect of the Charged State by Means of the  $\zeta$ -Potential.** One of the parameters to be studied was the influence of electrostatic interactions—or lack of them—during the growth process. To this end, we measured the charge of each ELR and polysaccharide prior to the QCM-D experiments by determining their  $\zeta$ -potentials at pH 4.0 and 5.5. The results are shown in Table 2. In the case of the polysaccharides, CHI exhibited a positive and ALG a negative charge as expected and, since both contain ionizable groups, their charge varied with the pH, with their potential decreasing at the pH value closest to their respective  $pK_a$  as their charges were progressively neutralized [close to the  $pK_a$  of ALG ( $\approx 3.2$ – $4$ )<sup>43</sup> and CHI ( $\approx 6$ ),<sup>25</sup> respectively]. As for the ELRs, it is interesting to note that, irrespective of the pH, in general they are all negatively



**Table 2.**  $\zeta$ -Potentials (mV) for CHI, ALG, and the ELRs at pH Values of 4.0 and 5.5

	pH 4.0	pH 5.5
3K-VRDG <sup>(-)</sup> V	$-2.7 \pm 0.6$	$-9.3 \pm 1.5$
3K-VRGDV	$-2.1 \pm 0.2$	$-8.4 \pm 0.3$
HAP3	$-0.4 \pm 0.8$	$-6.8 \pm 0.7$
GEG15	$-2.9 \pm 0.6$	$-4.4 \pm 0.4$
H3A20	$-13.3 \pm 1.7$	$-10.7 \pm 2.8$
IK24	$3.5 \pm 0.4$	$1.6 \pm 0.1$
H-RGD6	$1.8 \pm 0.1$	$-5.1 \pm 1.0$
H3A20H3	$-17.7 \pm 2.1$	$-15.0 \pm 2.6$
Neutralized V84	$1.1 \pm 0.8$	$-1.0 \pm 0.1$
CHI	$16.8 \pm 0.8$	$13.1 \pm 0.3$
ALG	$-8.3 \pm 1.0$	$-17.5 \pm 1.5$

charged despite the fact that all ELRs, except GEG15, have a higher proportion of residues that are susceptible of exhibiting a positive charge, with the highest being H-RGD6 (84.4%) and IK24 (96%), in comparison to the number of negative ones.

One would expect that some ELRs should exhibit positive values, especially at pH 4.0, where the availability of uncharged protonated COOH groups would be higher. The complexity of the ELR polypeptide family may explain why this did not occur: characteristics such as chain conformation and residue exhibition/inhibition may vary among different peptide sequences. Indeed, previous studies have shown that the  $pK_a$  of ionizable side-chains may change significantly, for example, with small changes in the amino acid sequence.<sup>44,45</sup> However, such a characterization was not in the scope of this work, since only the effective charge of each polymer in solution was considered when reaching the conclusions presented below. The IK24 and H-RGD6 ELRs are indeed positively charged at pH 4.0. In the case of the former, although it has an E-residue that can be ionized with a negative charge, the fact that the K-residues are in excess does not allow for a charge sign inversion below pH 5.5. A similar situation was found for neutralized V84, which contains no ionizable residues, although in this case the small charge fluctuation is due to the effect of pH on the N-

and C-termini. In contrast, the block-ELRs (H3A20 and H3A20H3) are more negative at pH 4.0 than at pH 5.5. Again, it is likely that a different conformation arises as a result of organization of the ELR into blocks and their amphiphilic nature.

Currently, two models are accepted to explain LbL growth driven by electrostatic interactions. One states that the LbL ingredients should have a minimum charge density with opposite signs, whereas the other states that, rather than having a minimum charge density, it is the charge balance that favors the buildup, i.e., that two ingredients are equally and symmetrically charged. Also, the gain of entropy can be hypothesized. For instance, it is known that, when using weak polyelectrolytes, polymers with a higher number of charged and polar groups tend to be adsorbed as a thin layer with a flat chain conformation whereas more neutral ones tend to be adsorbed as a thicker layer and to form loop-type structures.<sup>46–48</sup> Since the ELRs used herein are modified versions of the basic repeating block of elastin (some with charged amino acids) they would appear to be the ingredient with the most hydrophobic backbone rather than the polysaccharides, and thus have a higher contribute to the entropy mechanism due to the formation of loopier and interdigitated layers. Moreover, changing the pH of weak polyelectrolytes, namely, the polysaccharides used, will also vary their ionizable state, making them more charged or less charged. However, unlike the presence or absence of electrostatic charges, the real weight of the entropic gain in the LbL mechanism cannot be directly measured, and thus was left out of the discussion presented below. In light of the above, we defined 36 test conditions. Each condition is a combination of a polysaccharide (CHI or ALG) with one of the nine ELRs. Each one of these combinations was then studied at two pH values: 4.0 and 5.5, close to the  $pK_a$  of ALG and CHI, respectively. This allowed combinations containing fully charged/ionized or partially charged (near- $pK_a$  conditions) forms of polysaccharides with ELRs to be compared. For convenience, each permutation combining ELRs, and either ALG or CHI at pH 4.0 or 5.5 will henceforth

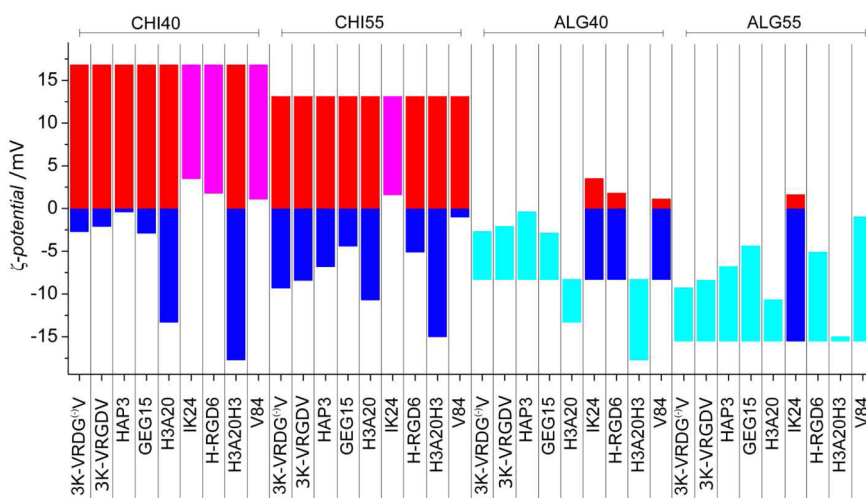


**Figure 1.** Range of  $\zeta$ -potentials for each polysaccharide/ELR combination. CHI40, CHI55, ALG40, and ALG55 represent combinations of CHI or ALG at pH 4.0 or pH 5.5. The division serves to indicate the charge balance between each polymer in terms of positive (red) and negative (blue) proportion of the whole bar length. Bars depicted in light blue and purple represent combinations in which both polymers exhibit potential with the same signal. For example, in the first column, where CHI and 3K-VRDG<sup>(-)</sup>V were used at pH 4.0, the  $\zeta$ -potentials were +16.8 mV and  $-2.7$  mV, respectively. In the last column, where ALG and V84 were used at pH 5.5, the  $\zeta$ -potentials were  $-15.5$  mV and  $-1$  mV, respectively.

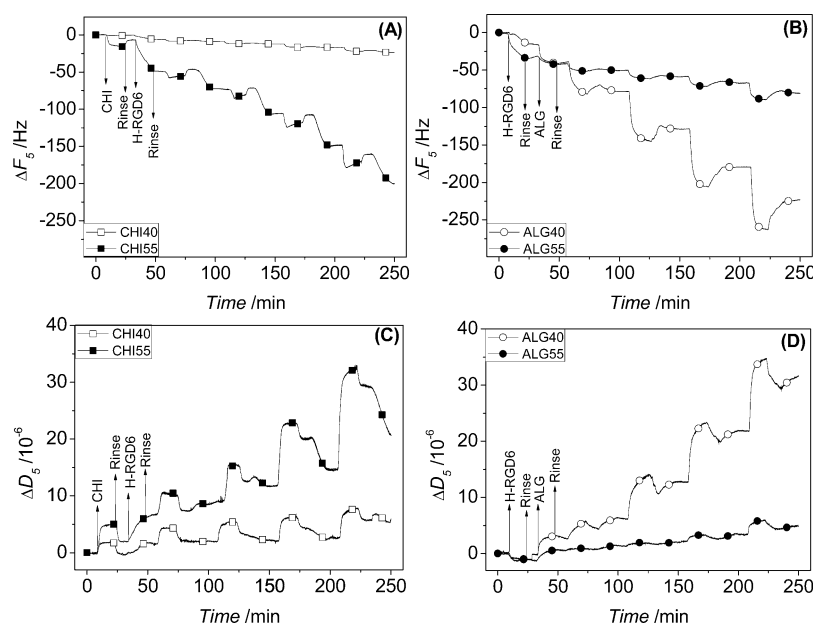


**Figure 2.** Representative QCM-D acquisition graphics depicting the fifth overtone variations of frequency (A, B) and dissipation (C, D) for hybrid polysaccharide/ELR films at pH 4.0 and 5.5. The case of H-RGD6 combinations is depicted. Results for CHI40 (□), CHI55 (■), ALG40 (○), and ALG55 (●) are shown. Absolute values of  $\Delta F$  and  $\Delta D$  reached values of (A) 24 Hz (□), 200 Hz (■); (B) 223 Hz (○), 81 Hz (●); (C)  $6 \times 10^{-6}$  (□),  $21 \times 10^{-6}$  (■); (D)  $32 \times 10^{-6}$  (○),  $5 \times 10^{-6}$  (●).

be referred to as ALG40 or CHI40 and ALG55 or CHI55, respectively.

Our first step was to represent graphically the  $\zeta$ -potentials of the polysaccharides and ELRs at each pH in Figure 1, in order to estimate the influence of the above-mentioned models. In this graphic, each end of the column represents the charge of each ingredient used in each of the 36 combinations. Lighter colors are used when the ingredients possess the same charge sign. First, identifying the potential combinations meeting the first ESA theory mentioned above is simple, since the only requirement is that the ingredients possess charge with opposite sign. Most CHI permutations meet the criteria, with only a few ALG ones. Second, we analyzed the charge balance under each condition. For CHI combinations, in general the  $\zeta$ -potential of the highly charged chitosan is not matched by the weakly charged ELRs under CHI40 conditions. This situation can be seen graphically by the different lengths of the bars on the positive and negative sides, or by bars represented in only one charge side. However, at pH 5.5, CHI becomes less charged ( $+13.1 \pm 0.3$  mV, in comparison to from  $+16.8 \pm 0.8$  mV) and at the same time the charge of the ELRs shifts to a more negatively charged state (notice that the charge of CHI and the block polypeptides H3A20 and H3A20H3 are balanced in either condition), thus leading to a more effective net charge balance. A similar trend is observed for ALG combinations. ALG at pH 4.0 is partially neutralized and the  $\zeta$ -potentials of the ELRs shift toward more positive values. This way, a more favorable electrostatic situation between ALG and ELRs is achieved but in a different manner than when using CHI: whereas with CHI55 balance is achieved by a decrease of its positive charge and an increase in the negative charge of the ELRs, with ALG40 a reduction in the electrostatic repulsion arising from a lower ionization state of ALG and the ELRs is observed, thereby representing a shift toward a situation where uncharged group interaction is maximized. Given the potential mechanisms at work under the different polysaccharide/ELR/pH permutations, we have resorted to the QCM-D in order to

determine the type of mechanism in which the construction of hybrid polysaccharide/ELR films majorly depends.

**QCM Data Acquisition.** Each experiment was conducted using a QCM-D to monitor the sequential adsorption of a single polysaccharide and an ELR. In each experiment, the pH of the solutions used (polymeric and rinsing) was adjusted to either 4.0 or 5.5. Also, in order to avoid the induction of conformational changes and data acquisition noise from the layers that had assembled previously, the pH values of the solutions used in each experiment were adjusted to the same value. Typical graphs of frequency ( $\Delta F$ ) and dissipation ( $\Delta D$ ) variations are depicted for five bilayers of CHI/ELR (Figure 2A and C, respectively) and ELR/ALG (Figure 2B and D, respectively) at different pH values. The example presented (the combinations using H-RGD6) shows the data obtained for the fifth overtone, which corresponds to an excitation frequency of 25 MHz, and is representative of all 36 polysaccharide/ELR/pH conditions. The graphics obtained for each combination studied can be found in Figure S3. During QCM-D acquisition, a favorable and successful construction is usually identified by a decrease in  $\Delta F$  caused by mass adsorption at the surface of the gold-coated quartz sensor.

At the same time, monitoring of  $\Delta D$  gives an indirect indication of the film's viscoelastic properties. For instance, an increase in  $\Delta D$  represents a shift toward a film with a higher viscous component and damping properties that becomes "softer", which is typical of polymeric LbL films. The dissipation values for a soft film are higher due to increased energy loss from the crystal, whereas smaller dissipation values are obtained for a rigid film. It is this dampening to the crystal's oscillation that is registered as dissipation ( $\Delta D$ ).<sup>49,50</sup> A closer look at Figure 2 allows the most favorable conditions for LbL construction of these hybrid films to be identified, namely, pH values close to the  $pK_a$  of the polysaccharide used, i.e., conditions ALG40 and CHI55, with absolute  $\Delta F_5$  values of around 225 and 200 Hz, respectively. Under these conditions,

the amplitude of  $\Delta F$  is greater than for the others. A similar trend is observed for  $\Delta D$ .

**Data Modeling and Thickness Analysis.** The data acquired allowed the thickness of the films obtained under each of the 36 conditions to be estimated. When constructing rigid films, the frequency values are related to the adsorbed film mass ( $\Delta m$ ) and that mass is directly related to  $\Delta F$ , a relation that is given by the well-known Sauerbrey equation:

$$\Delta m = -\frac{C \times \Delta F}{n} \quad (1)$$

where  $C$  is the mass sensitivity constant and  $n$  is the overtone number. However, this relation cannot be used for soft films that exhibit viscoelastic properties since the water content and swelling behavior are also reflected in  $\Delta F$  and must be taken into account. Therefore, in order to compare every combination in this study, the obtained frequency and dissipation values were converted to their estimated thickness using the Voigt-based viscoelastic model,<sup>51</sup> which is integrated into the QTools software from Q-Sense, based on eqs 2 and 3:

$$\Delta F \approx -\frac{1}{2\pi\rho_0 h_0} \left\{ \frac{\eta_3}{\delta_3} + \sum_{j=k} \left[ h_j \rho_j \omega - 2h_j \left( \frac{\eta_3}{\delta_3} \right)^2 \frac{\eta_j \omega^2}{\mu_j^2 + \omega^2 \eta_j^2} \right] \right\} \quad (2)$$

$$\Delta D \approx \frac{1}{2\pi f \rho_0 h_0} \left\{ \frac{\eta_3}{\delta_3} + \sum_{j=k} \left[ 2h_j \left( \frac{\eta_3}{\delta_3} \right)^2 \frac{\mu_j \omega}{\mu_j^2 + \omega^2 \eta_j^2} \right] \right\} \quad (3)$$

where, considering a total of  $k$  thin viscoelastic layers,  $\rho_0$  and  $h_0$  are the density and thickness of the quartz crystal,  $\eta_3$  is the viscosity of the bulk liquid,  $\delta_3$  is the viscous penetration depth of the shear wave in the bulk liquid,  $\rho_3$  is the density of liquid,  $\mu$  is the elastic shear modulus of an overlayer, and  $\omega$  is the angular frequency of the oscillation. Together with the integrated Voigt-based viscoelastic model, QCM-D constitutes a technique that is both precise and simple to use, allowing one to obtaining a film's properties quickly when comparing to other techniques, such as ellipsometry and surface plasmon spectroscopy. The thickness results can be found in Figure 3. Also, the numerical thickness and  $\chi^2$  values associated with the model fitting can be found in Figure S3 in the Supporting Information.

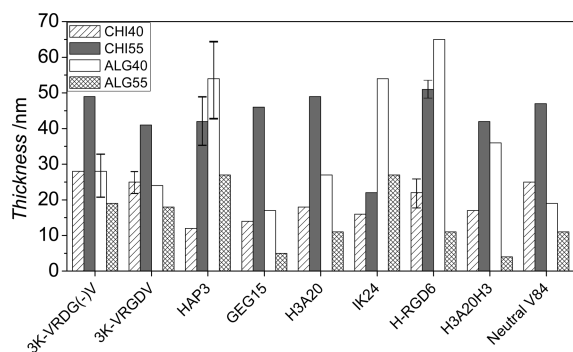


**Figure 3.** Thickness values for multilayered films containing five bilayers, as estimated using the Voigt-based viscoelastic model, for each polysaccharide/ELR permutation at pH 4.0 and pH 5.5. Deviation bars represent two standard deviations.

The results for CHI and ALG combinations were subsequently analyzed separately in order to avoid an analysis of construction mechanisms that cannot be solely explained by the thickness and potential but are also influenced by the specific nature of the polymer itself.

In LbL growth, different materials tend to adsorb with distinct kinetics and conformations, thus meaning that, although both CHI and ALG are polysaccharides, they will react differently with ELRs in a multilayer hybrid film. The series plotted in Figure 3 represent the results obtained when using ALG at pH 4.0 or pH 5.5 and CHI at the same pH values. Some combinations were performed in triplicate, leading to an estimated maximum standard error of 12% (estimated from HAP3 at ALG40).

First it can be seen that the overall thickness values are higher for combinations containing CHI as the polysaccharide: the sum of all thickness values for CHI is 566 nm, while that for ALG is 456 nm. If we consider solely the role of ESA interactions, the overall construction of the films is more favorable with CHI than when using ALG, since the former is a polycation and most ELRs are negatively charged. For films made of H-RGD6, IK24, and HAP3, ALG40 conditions are actually more favorable than CHI55, but this observation can be explained by their exhibited charge, with the first two being positive at pH 4.0 (1.8 and 3.5 mV, respectively) whereas the third is nearly neutral (−0.4 mV). The overall construction phenomenon looks dependent on the charge sign among the ingredients. However, it should be noted that the analysis resulting from Figure 1 shows that most ALG/pH permutations do not meet the criteria to follow a construction based on a minimum charge density, i.e., the ingredients do not possess opposite charge sign and the ingredients are all negatively charged. Despite this fact, LbL was still possible when using ALG and thus the mechanism of construction must depend on additional factors. A more specific look at each polysaccharide combination will allow further data to be obtained regarding the growth mechanism at work.

When analyzing the CHI and ALG combinations separately, another trend was identified. For each polysaccharide/ELR condition, the thickness is higher when the polysaccharides were only partially charged, i.e., at near- $pK_a$  conditions. Following again the example of H-RGD6, for instance, the thickness of films at CHI40 and CHI55 conditions were 22 and 51 nm, whereas at ALG40 and ALG 55 they were 65 and 11 nm, respectively. In the case of CHI/ELR films, the model of charge balance and symmetry alone could explain the construction mechanism, but for ALG permutations such model is not valid, as denoted above. At pH 4.0, there is less electrostatic repulsion between ALG and ELRs are electrostatically more balanced than at pH 5.5. The fact that the majority of permutations involve ingredients with the same charge sign means there is no charge symmetry, and thus also conflict with the charge balance model. This result suggests that the proposed hybrid multilayer construction depends on a lower charge density of the polysaccharides, regardless of charge sign, by increasing the availability of neutral binding sites, and therefore, materials with a low charge density are a key factor for the construction of polysaccharide/ELR films. In this case, we hypothesize that secondary hydrophobic interactions are a key force driving LbL growth. The block-ELRs H3A20 and H3A20H3 are a good example of this mechanism. As observed in Figure 1, these polymers are electrostatically well-balanced with CHI at both pH values (CHI40/H3A20: +16.8/−13.3

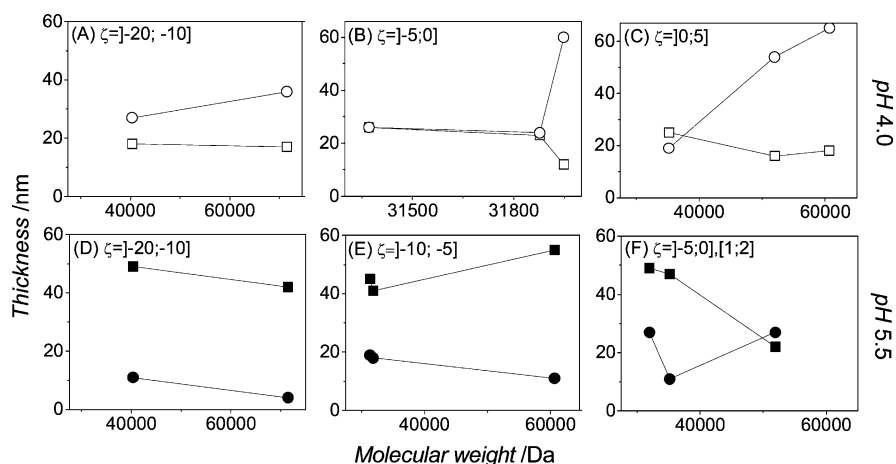


**Figure 4.** Variations in film thickness with ELR molecular weight sorted by pH and  $\zeta$ -potential. Results for CHI40 ( $\square$ ), CHI55 ( $\blacksquare$ ), ALG40 ( $\circ$ ), and ALG55 ( $\bullet$ ) are shown. The mean thickness of 3K-VRDG<sup>(-)</sup>V and 3K-VRGDV films ( $M_n = 31371$  Da) is represented.

mV; CHI55/H3A20: +13.1/−10.7 mV; CHI40/H3A20H3: +16.8/−17.7 mV; CHI55/H3A20H3: +13.1/−15.0 mV). Although their  $\zeta$ -potentials would favor ESA balance in both cases, thicknesses are higher at CHI55 than at CHI40, where the availability of charged groups is lower in comparison. To further consolidate this observation, we have also studied the growth mechanism with the neutralized V84, which has no ionizable groups. It is noteworthy that favorable LbL growth under near- $pK_a$  conditions is also observed for this ELR. Therefore, whereas ESA interactions are present in all other ELRs, the successful construction of polysaccharide/(neutralized V84) films relies solely on the density of hydrophobic groups under ALG40 and CHI55 conditions.

**Effect of Molecular Weight.** Due to the complexity of the ELR samples tested, several parameters, namely, molecular weight, pH, zeta-potential, charge density, and charge balance between each film component, must be considered to determine their contribution to film growth. In this regard, we have tested the obtained data against these parameters assuming that hydrophobic forces play an important role in the self-assembly process. First of all, we plotted thickness as a function of the  $\zeta$ -potential and molecular weight ( $M_n$ ) of the ELRs for each set of polysaccharide/pH combinations. The variations of thickness with  $\zeta$ -potential (Figure S2A) and  $M_n$  (Figure S2B) are represented, which shows no clear trend in either case.

At this point, it was assumed that ELRs with a similar  $M_n$  exhibit different potentials, and vice versa. For instance, 3K-VRGDV ( $M_n = 31371$  Da) has a charge of  $-8.4 \pm 0.3$  mV at pH 5.5, whereas another ELR with very similar  $M_n$  like neutralized V84 ( $M_n = 35191$  Da) has a charge of only  $-1.0 \pm 0.1$  mV. The ELRs were therefore grouped according to their mean charge and their thickness plotted as a function of  $M_n$  for each defined charge range (see Figure 4).

In general, one would expect that a higher  $M_n$  would lead to a thicker film. Thus, whereas a small molecule adsorbs in an extended conformation, a lengthier polymer tends to adsorb in a more “loopier” manner, thereby providing more anchoring sites for the next layer to adsorb and, potentially, higher interpenetration capabilities than smaller ones.<sup>52</sup> For each  $\zeta$ -potential range selected, the use of fully charged polysaccharides (ALG55 and CHI40) leads to a thickness decrease with increasing  $M_n$ . Under near- $pK_a$  conditions of ALG, the overall thickness of the films increases with  $M_n$ . However, this

observation was valid for all ALG40 combinations but not all CHI55 ones, with three of the 36 conditions tested being atypical. It can be seen from Figure 4D that the thickness under CHI55 conditions decreases from 49 to 42 nm. The ELR in question is H3A20H3 ( $M_n = 71462$  Da), which is organized into two charged blocks separated by another nonpolar block of alanine residues (A). We therefore hypothesize that, during LbL growth, the charged blocks are the first to contact with the underlying surface whereas the highly neutral and nonpolar block containing a high number of A-residues (hydropathy index of 1.8)<sup>53</sup> is much less likely to interact with the hydrated film. Although it is true that all ELRs possess hydrophobic residues in their backbone, block-ELRs are spatially organized with one block completely charge-free, thus limiting its interaction with aqueous solvents.

The other two anomalous situations can be seen in Figure 4F. The first, at CHI55 for IK24 ( $M_n = 51970$  Da), shows a thickness decrease to 22 nm. IK24 exhibits the highest percentage of positively ionizable residues. As such, even when CHI is only partially deprotonated, it is plausible to assume that the positive charges of both ingredients (which are stronger and longer in range) repel, thereby minimizing the interaction between shorter range hydrophobic groups. The second, at ALG55 for the same ELR, shows a thickness increase to 27 nm. Under these conditions, the positively charged IK24 may interact well with ALG as a result of ESA interactions. Note that these  $M_n$ -dependent exceptions do not conflict with the fact that, for each polysaccharide/ELR combination, adsorption is more favorable under near- $pK_a$  conditions: ALG55 is still a less favorable condition than ALG40, even for the polycationic IK24.

It is unclear why the trend in this behavior does not completely match the molecular weight model for LbL assembly and is distinct among many of the studied conditions. Therefore, in light of the uncertain influence of  $M_n$  on multilayer construction, the fact that it is only favorable in specific cases leads to the conclusion that it is not a primary influence on the growth mechanism.

**General Model for Hybrid Multilayer Growth.** We have shown that a shift toward near- $pK_a$  conditions for both polysaccharides, although of different nature, favors the construction of hybrid nanostructured polysaccharide/ELR films. The same arguments rule out the theory of minimum charge density, since LbL growth is observed even when



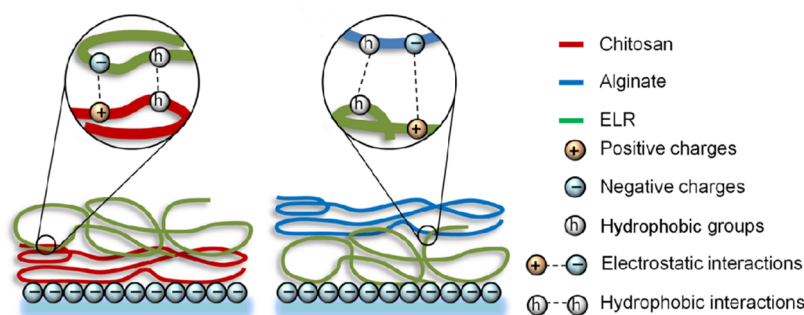


**Figure 5.** Representative scheme of the hypothetical interactions occurring between polysaccharides and ELRs.

charges of the same sign are present. Based on this extensive analysis, the LbL growth of hybrid polysaccharide and ELR films cannot be explained by ESA interactions alone, thus meaning that secondary hydrophobic interactions must be taken into account. The arguments presented herein are also valid for the control ELR (neutralized V84). As this ELR exhibits no ionizable groups, the construction of films with neutralized V84 was also more favorable under near- $pK_a$  conditions, thus further clarifying the role of nonelectrostatic forces. A schematic depiction of our findings is provided in Figure 5.

## CONCLUSION

The contributions of the molecular weight and electrostatic and hydrophobic interactions to LbL film growth have been extensively studied using a QCM-D method. Thus, a comparison of the thickness of 36 films formed under different conditions (polysaccharide and ELR combinations and the charges of each intervening ingredient) has shown that the growth of such hybrid nanostructured films is more favorable when the polysaccharide used is partially neutral, i.e., near its  $pK_a$ . Under these conditions, hydrophobic groups prevail over charged ones, thus highlighting the greater importance of short-range hydrophobic interactions when compared with ESA interactions. The molecular weight appears to have little effect on LbL growth. Future studies that focus on other parameters, such as ionic strength and temperature, should be considered in order to determine whether additional factors affect this combination model. These conclusions are important in order to correctly predict the most favorable parameters for constructing nanostructured films from natural and nature-inspired materials, especially since the use of genetically engineered polypeptides could lead to films with tailored properties and biologically relevant functions for applications in tissue engineering, drug delivery, and biotechnology that require precise and improved specificity.

## ASSOCIATED CONTENT

### Supporting Information

Neutralization of V84. Detailed MALDI-TOF and amino acid composition experimental results.  $\zeta$ -potential and molecular weight effect on thickness. QCM-D data acquired during film growth and Voigt-based viscoelastic model fitting results. Complete list of authors of refs 6 and 22. This material is available free of charge via the Internet at <http://pubs.acs.org>.

## AUTHOR INFORMATION

### Corresponding Author

\*E-mail: [jmano@dep.uminho.pt](mailto:jmano@dep.uminho.pt).

## Author Contributions

The manuscript was written through contributions of all authors. All authors have given approval to the final version of the manuscript.

## Notes

The authors declare no competing financial interest.

## ACKNOWLEDGMENTS

This work was carried out under the scope of Fundação para a Ciência e Tecnologia – FCT (grant SFRH/BD/61126/2009), “Fundo Social Europeu” – FSE, “Programa Diferencial de Potencial Humano” – POPH, EU 7th Framework Programme (n° REGPOT-CT2012-316331-POLARIS), the MICINN (MAT 2009 14195-C03 03, ACI2009-0890, MAT2010-15310, MAT2010-15982 and PRI-PIBAR-2011-1403), the JCyL (VA049A11, VA152A12 and VA155A12), the CIBER-BBN and the E.C.

## REFERENCES

- (1) Hook, A. L.; Voelcker, N. H.; Thissen, H. Patterned and Switchable Surfaces for Biomolecular Manipulation. *Acta Biomater.* **2009**, *5*, 2350–2370.
- (2) Prakash, S.; Karacor, M. B.; Banerjee, S. Surface Modification in Microsystems and Nanosystems. *Surf. Sci. Rep.* **2009**, *64*, 233–254.
- (3) Tirrell, M.; Kokkoli, E.; Biesalski, M. The Role of Surface Science in Bioengineered Materials. *Surf. Sci.* **2002**, *500*, 61–83.
- (4) Alves, N. M.; Pashkuleva, I.; Reis, R. L.; Mano, J. F. Controlling Cell Behavior Through the Design of Polymer Surfaces. *Small* **2010**, *6*, 2208–2220.
- (5) Boudou, T.; Crouzier, T.; Ren, K.; Blin, G.; Picart, C. Multiple Functionalities of Polyelectrolyte Multilayer Films: New Biomedical Applications. *Adv. Mater.* **2010**, *22*, 441–467.
- (6) Stuart, M. A. C.; Huck, W. T. S.; Genzer, J.; Muller, M.; Ober, C.; Stamm, M.; Sukhorukov, G. B.; Szleifer, I.; Tsukruk, V. V.; Urban, M.; et al. Emerging Applications of Stimuli-Responsive Polymer Materials. *Nat. Mater.* **2010**, *9*, 101–113.
- (7) Wong, J. E.; Müller, C. B.; Laschewsky, A.; Richtering, W. Direct Evidence of Layer-by-Layer Assembly of Polyelectrolyte Multilayers on Soft and Porous Temperature-Sensitive PNIPAM Microgel Using Fluorescence Correlation Spectroscopy. *J. Phys. Chem. B* **2007**, *111*, 8527–8531.
- (8) Gribova, V.; Auzely-Velty, R.; Picart, C. Polyelectrolyte Multilayer Assemblies on Materials Surfaces: From Cell Adhesion to Tissue Engineering. *Chem. Mater.* **2012**, *24*, 854–869.
- (9) Silva, H. S.; Miranda, P. B. Molecular Ordering of Layer-by-Layer Polyelectrolyte Films Studied by Sum-Frequency Vibrational Spectroscopy. *J. Phys. Chem. B* **2009**, *113*, 10068–10071.
- (10) Tang, Z.; Wang, Y.; Podsiadlo, P.; Kotov, N. A. Biomedical Applications of Layer-by-Layer Assembly: From Biomimetics to Tissue Engineering. *Adv. Mater.* **2006**, *18*, 3203–3224.



- (11) Martins, G. V.; Mano, J. F.; Alves, N. M. Dual Responsive Nanostructured Surfaces for Biomedical Applications. *Langmuir* **2011**, *27*, 8415–8423.
- (12) Zahn, R.; Thomasson, E.; Guillaume-Gentil, O.; Vörös, J.; Zambelli, T. Ion-Induced Cell Sheet Detachment from Standard Cell Culture Surfaces Coated with Polyelectrolytes. *Biomaterials* **2012**, *33*, 3421–3427.
- (13) Manna, U.; Patil, S. Borax Mediated Layer-by-Layer Self-Assembly of Neutral Poly(vinyl alcohol) and Chitosan. *J. Phys. Chem. B* **2009**, *113*, 9137–9142.
- (14) Rivera-Gil, P.; De Koker, S.; De Geest, B. G.; Parak, W. J. Intracellular Processing of Proteins Mediated by Biodegradable Polyelectrolyte Capsules. *Nano Lett.* **2009**, *9*, 4398–4402.
- (15) Volodkin, D. V.; Madaboosi, N.; Blacklock, J.; Skirtach, A. G.; Möhwald, H. Surface-Supported Multilayers Decorated with Bio-active Material Aimed at Light-Triggered Drug Delivery. *Langmuir* **2009**, *25*, 14037–14043.
- (16) Sher, P.; Custodio, C. A.; Mano, J. F. Layer-By-Layer Technique for Producing Porous Nanostructured 3D Constructs Using Moldable Freeform Assembly of Spherical Templates. *Small* **2010**, *6*, 2644–2648.
- (17) Decher, G.; Hong, J. D.; Schmitt, J. Buildup of Ultrathin Multilayer Films by a Self-Assembly Process: III. Consecutively Alternating Adsorption of Anionic and Cationic Polyelectrolytes on Charged Surfaces. *Thin Solid Films* **1992**, *210–211*, 831–835.
- (18) Hammond, P. T. Form and Function in Multilayer Assembly: New Applications at the Nanoscale. *Adv. Mater.* **2004**, *16*, 1271–1293.
- (19) Lyklema, J.; Deschênes, L. The First Step in Layer-by-Layer Deposition: Electrostatics and/or Non-Electrostatics? *Adv. Colloid Interface Sci.* **2011**, *168*, 135–148.
- (20) Klitzing, V. R. Internal Structure of Polyelectrolyte Multilayer Assemblies. *Phys. Chem. Chem. Phys.* **2006**, *8*, 5012–5033.
- (21) Dubas, S. T.; Schlenoff, J. B. Factors Controlling the Growth of Polyelectrolyte Multilayers. *Macromolecules* **1999**, *32*, 8153–8160.
- (22) Mano, J. F.; Silva, G. A.; Azevedo, H. S.; Malafaya, P. B.; Sousa, R. A.; Silva, S. S.; Boesel, L. F.; Oliveira, J. M.; Santos, T. C.; Marques, A. P.; et al. Natural Origin Biodegradable Systems in Tissue Engineering and Regenerative Medicine: Present Status and Some Moving Trends. *J. R. Soc. Interface* **2007**, *4*, 999–1030.
- (23) Boateng, J. S.; Matthews, K. H.; Stevens, H. N. E.; Eccleston, G. M. Wound Healing Dressings and Drug Delivery Systems: A Review. *J. Pharm. Sci.* **2008**, *97*, 2892–2923.
- (24) George, M.; Abraham, T. E. Polyionic Hydrocolloids for the Intestinal Delivery of Protein Drugs: Alginate and Chitosan — A Review. *J. Controlled Release* **2006**, *114*, 1–14.
- (25) Rinaudo, M. Chitin and Chitosan - Properties and Applications. *Prog. Polym. Sci.* **2006**, *31*, 603–632.
- (26) Almine, J. F.; Bax, D. V.; Mithieux, S. M.; Nivison-Smith, L.; Rnjak, J.; Waterhouse, A.; Wise, S. G.; Weiss, A. S. Elastin-Based Materials. *Chem. Soc. Rev.* **2010**, *39*, 3371–3379.
- (27) Rodríguez-Cabello, J. C.; Martín, L.; Alonso, M.; Arias, F. J.; Testera, A. M. "Recombinamers" as Advanced Materials for the Post-Oil Age. *Polymer* **2009**, *50*, 5159–5169.
- (28) Urry, D. W. Molecular Machines: How Motion and Other Functions of Living Organisms Can Result from Reversible Chemical Changes. *Angew. Chem., Int. Ed.* **1993**, *32*, 819–841.
- (29) Costa, R. R.; Custódio, C. A.; Arias, F. J.; Rodríguez-Cabello, J. C.; Mano, J. F. Layer-by-Layer Assembly of Chitosan and Recombinant Biopolymers into Biomimetic Coatings with Multiple Stimuli-Responsive Properties. *Small* **2011**, *7*, 2640–2649.
- (30) Nettles, D. L.; Chilkoti, A.; Setton, L. A. Applications of Elastin-Like Polypeptides in Tissue Engineering. *Adv. Drug Delivery Rev.* **2010**, *62*, 1479–1485.
- (31) Prieto, S.; Shkilnyy, A.; Rumlach, C.; Ribeiro, A.; Arias, F. J.; Rodríguez-Cabello, J. C.; Taubert, A. Biomimetic Calcium Phosphate Mineralization with Multifunctional Elastin-Like Recombinamers. *Biomacromolecules* **2011**, *12*, 1480–1486.
- (32) Cini, N.; Tulun, T.; Decher, G.; Ball, V. Step-by-Step Assembly of Self-Patterning Polyelectrolyte Films Violating (Almost) All Rules of Layer-by-Layer Deposition. *J. Am. Chem. Soc.* **2010**, *132*, 8264–8265.
- (33) Garg, A.; Heflin, J. R.; Gibson, H. W.; Davis, R. M. Study of Film Structure and Adsorption Kinetics of Polyelectrolyte Multilayer Films: Effect of pH and Polymer Concentration. *Langmuir* **2008**, *24*, 10887–10894.
- (34) Liu, H.; Hu, N. Interaction between Myoglobin and Hyaluronic Acid in Their Layer-by-Layer Assembly: Quartz Crystal Microbalance and Cyclic Voltammetry Studies. *J. Phys. Chem. B* **2006**, *110*, 14494–14502.
- (35) Marx, K. A. Quartz Crystal Microbalance: A Useful Tool for Studying Thin Polymer Films and Complex Biomolecular Systems at the Solution–Surface Interface. *Biomacromolecules* **2003**, *4*, 1099–1120.
- (36) Molino, P. J.; Higgins, M. J.; Innis, P. C.; Kapsa, R. M. I.; Wallace, G. G. Fibronectin and Bovine Serum Albumin Adsorption and Conformational Dynamics on Inherently Conducting Polymers: A QCM-D Study. *Langmuir* **2012**, *28*, 8433–8445.
- (37) Weber, N.; Pesnell, A.; Bolikal, D.; Zeltinger, J.; Kohn, J. Viscoelastic Properties of Fibrinogen Adsorbed to the Surface of Biomaterials Used in Blood-Contacting Medical Devices. *Langmuir* **2007**, *23*, 3298–3304.
- (38) Hirai, A.; Odani, H.; Nakajima, A. Determination of Degree of Deacetylation of Chitosan by <sup>1</sup>H NMR Spectroscopy. *Polym. Bull.* **1991**, *26*, 87–94.
- (39) Dutta, A. K.; Belfort, G. Adsorbed Gels versus Brushes: Viscoelastic Differences. *Langmuir* **2007**, *23*, 3088–3094.
- (40) Caruso, F.; Niikura, K.; Furlong, D. N.; Okahata, Y. 2. Assembly of Alternating Polyelectrolyte and Protein Multilayer Films for Immunosensing. *Langmuir* **1997**, *13*, 3427–3433.
- (41) Gergely, C.; Bahi, S.; Szalontai, B.; Flores, H.; Schaaf, P.; Voegel, J.-C.; Cuisinier, F. J. G. Human Serum Albumin Self-Assembly on Weak Polyelectrolyte Multilayer Films Structurally Modified by pH Changes. *Langmuir* **2004**, *20*, 5575–5582.
- (42) Houska, M.; Brynda, E. Interactions of Proteins with Polyelectrolytes at Solid/Liquid Interfaces: Sequential Adsorption of Albumin and Heparin. *J. Colloid Interface Sci.* **1997**, *188*, 243–250.
- (43) Ju, H. K.; Kim, S. Y.; Lee, Y. M. pH/Temperature-Responsive Behaviors of Semi-IPN and Comb-Type Graft Hydrogels Composed of Alginate and Poly(N-Isopropylacrylamide). *Polymer* **2001**, *42*, 6851–6857.
- (44) Urry, D. W.; Hayes, L. C.; Gowda, D. C.; Peng, S. Q.; Jing, N. J. Electrochemical Transduction in Elastic Protein-Based Polymers: A Model for an Energy Conversion Step of Oxidative Phosphorylation. *Biochem. Biophys. Res. Commun.* **1995**, *210*, 1031–1039.
- (45) Urry, D. W.; Peng, S.; Gowda, D. C.; Parker, T. M.; Harris, R. D. Comparison of Electrostatic- and Hydrophobic-Induced pKa Shifts in Polypeptides. The Lysine Residue. *Chem. Phys. Lett.* **1994**, *225*, 97–103.
- (46) Burke, S. E.; Barrett, C. J. pH-Responsive Properties of Multilayered Poly(L-Lysine)/Hyaluronic Acid Surfaces. *Biomacromolecules* **2003**, *4*, 1773–1783.
- (47) Fu, J.; Ji, J.; Yuan, W.; Shen, J. Construction of Anti-Adhesive and Antibacterial Multilayer Films via Layer-by-Layer Assembly of Heparin and Chitosan. *Biomaterials* **2005**, *26*, 6684–6692.
- (48) Yoo, D.; Shiratori, S. S.; Rubner, M. F. Controlling Bilayer Composition and Surface Wettability of Sequentially Adsorbed Multilayers of Weak Polyelectrolytes. *Macromolecules* **1998**, *31*, 4309–4318.
- (49) Cho, N.-J.; Kanazawa, K. K.; Glenn, J. S.; Frank, C. W. Employing Two Different Quartz Crystal Microbalance Models To Study Changes in Viscoelastic Behavior upon Transformation of Lipid Vesicles to a Bilayer on a Gold Surface. *Anal. Chem.* **2007**, *79*, 7027–7035.
- (50) Höök, F.; Kasemo, B.; Nylander, T.; Fant, C.; Sott, K.; Elwing, H. Variations in Coupled Water, Viscoelastic Properties, and Film Thickness of a Mefp-1 Protein Film during Adsorption and Cross-Linking: A Quartz Crystal Microbalance with Dissipation Monitoring,

Ellipsometry, and Surface Plasmon Resonance Study. *Anal. Chem.* **2001**, *73*, 5796–5804.

(51) Voinova, M. V.; Rodahl, M.; Jonson, M.; Kasemo, B. Viscoelastic Acoustic Response of Layered Polymer Films at Fluid-Solid Interfaces: Continuum Mechanics Approach. *Phys. Scr.* **1999**, *59*, 391–396.

(52) Kujawa, P.; Moraille, P.; Sanchez, J.; Badia, A.; Winnik, F. M. Effect of Molecular Weight on the Exponential Growth and Morphology of Hyaluronan/Chitosan Multilayers: A Surface Plasmon Resonance Spectroscopy and Atomic Force Microscopy Investigation. *J. Am. Chem. Soc.* **2005**, *127*, 9224–9234.

(53) Kyte, J.; Doolittle, R. F. A Simple Method for Displaying the Hydropathic Character of a Protein. *J. Mol. Biol.* **1982**, *157*, 105–132.